nanomaterials

MDPI

Article

Impact of Proton Irradiation on Medium Density Polyethylene/Carbon Nanocomposites for Space Shielding Applications

Federica Zaccardi [1,†], Elisa Toto [2,†], Shreya Rastogi [3], Valeria La Saponara [3], Maria Gabriella Santonicola [2] and Susanna Laurenzi [1,*]

[1] Department of Astronautical Electrical and Energy Engineering, Sapienza University of Rome, Via Salaria 851-881, 00138 Rome, Italy
[2] Department of Chemical Engineering Materials Environment, Sapienza University of Rome, Via del Castro Laurenziano 7, 00161 Rome, Italy; elisa.toto@uniroma1.it (E.T.); mariagabriella.santonicola@uniroma1.it (M.G.S.)
[3] Department of Mechanical and Aerospace Engineering, University of California Davis, One Shields Ave, Davis, CA 95616, USA; vlasaponara@ucdavis.edu (V.L.S.)
* Correspondence: susanna.laurenzi@uniroma1.it
† These authors contributed equally to this work.

Abstract: The development of novel materials with improved radiation shielding capability is a fundamental step towards the optimization of passive radiation countermeasures. Polyethylene (PE) nanocomposites filled with carbon nanotubes (CNT) or graphene nanoplatelets (GNP) can be a good compromise for maintaining the radiation shielding properties of the hydrogen-rich polymer while endowing the material with multifunctional properties. In this work, nanocomposite materials based on medium-density polyethylene (MDPE) loaded with different amounts of multi-walled carbon nanotubes (MWCNT), GNPs, and hybrid MWCNT/GNP nanofillers were fabricated, and their properties were examined before and after proton exposure. The effects of irradiation were evaluated in terms of modifications in the chemical and physical structure, wettability, and surface morphology of the nanocomposites. The aim of this work was to define and compare the MDPE-based nanocomposite behavior under proton irradiation in order to establish the best system for applications as space shielding materials.

Keywords: radiation shielding ability; polyethylene nanocomposites; space environmental degradation; proton irradiation; surface analysis

Citation: Zaccardi, F.; Toto, E.; Rastogi, S.; La Saponara, V.; Santonicola, M.G.; Laurenzi, S. Impact of Proton Irradiation on Medium Density Polyethylene/Carbon Nanocomposites for Space Shielding Applications. *Nanomaterials* **2023**, *13*, 1288. https://doi.org/10.3390/nano13071288

Academic Editor: Giancarlo Rizza

Received: 25 February 2023
Revised: 1 April 2023
Accepted: 4 April 2023
Published: 6 April 2023

1. Introduction

Polyethylene (PE) is a widely researched material that finds application in different fields due to its low weight, low cost, and easy processability. Its high biocompatibility, good mechanical properties, and chemical resistance have made PE the material of choice for the commercial production of orthopedic prostheses and packaging [1,2]. In the space sector, PE and PE-based composites are used as a barrier against the hazardous space radiation environment [3,4]. In fact, it is widely recognized that materials composed of low atomic number atoms offer protection against radiation [5]. PE is composed of the ethylene monomer –[CH_2–CH_2]– with high content of H atoms and is, therefore, the solid material with the most efficient radiation shielding properties [6]. However, PE is a dielectric polymer and does not possess enough strength and thermal stability to be considered as a structural material [5]. For this reason, carbon nanoparticles are widely investigated for the fabrication of novel PE nanocomposite materials with potentially enhanced mechanical and functional properties: high electrical conductivity for static charge dissipation, high thermal conductivity, radiation hardness, and mechanical integrity [5–10]. Many investigations have been reported on the multifunctional properties of nanocomposites based on

PE loaded with graphene nanoplatelets (GNP) or carbon nanotubes (CNT), where the PE matrix takes advantage of the exceptionally high strength-to-weight ratio and of the high thermal and electrical conductivities of carbon nanoparticles [11–13]. Moreover, several studies report on the effects of different types of irradiation on PE and carbon-filled PE composites, including cross-linking, chain scissions, formation of free radicals, and release of hydrogen [14–17]. Nevertheless, if the effects of radiation on PE are well-known, studies on the response to radiation of CNTs and GNPs have been limited. However, several studies report applications of graphene/polymer nanocomposites for radiation sensing [18–22], exploiting the high electrical conductivity of the carbon filler. The numerical and experimental studies conducted so far indicate that CNTs are radiation-tolerant nanoparticles [23,24]. The current literature suggests possible beneficial effects of radiation that lead to the formation of inter-tube covalent bonds and of stable cross-links between neighboring CNTs within bundles, thus eliminating the sliding between the nanotubes and increasing their mechanical properties [25,26]. Regarding CNTs nanocomposites, a beneficial effect of the nanoparticles has been observed by many authors [27–30]. The experimental results on the effects of different types of radiation showed that the addition of CNTs can improve the shielding ability of the polymeric matrices [27–30]. Wilkins et al. [31] investigated, using Raman spectroscopy, the effects of different simulated space radiation environments on PE loaded with raw (non-functionalized) and functionalized single-walled carbon nanotubes (SWCNT). Results showed that SWCNTs are highly radiation tolerant to space radiation environments, but further studies with additional experimental techniques must be implemented to understand the mechanisms of material–radiation interactions. Contrary to CNTs, studies on the effects of different radiation sources on GNPs report the formation of topological defects such as the ejection of multiple atoms and consequent formation of vacancies [32,33]. However, improvement of radiation resistance, less crystal defects and self-healing mechanism of radiation-induced defects are also observed in GNP nanocomposites by many authors [34–38]. Overall, only few experiments with preliminary results have been conducted to investigate the radioprotectant properties of carbon-based polymer nanocomposites, and the impact of radiation on PE nanocomposites is still unknown.

In this work, nanocomposite materials based on medium-density polyethylene (MDPE) loaded with different amounts of multi-walled carbon nanotubes (MWCNT), GNPs, and hybrid MWCNT/GNP nanofillers are fabricated by a molding technique. The nanocomposites are investigated in terms of chemical structure, thermal behavior, wettability, and morphology, before and after proton irradiation. Results are useful to guide the application of these materials in space environments characterized by high levels of ionizing radiation.

2. Materials and Methods

Medium-density polyethylene (MDPE) in the form of powder was supplied by Sigma Aldrich (product code 332119, density 0.94 g/cm^3) and used as received. Exfoliated graphene nanoplatelets of grade C750 (thickness ~2 nm, average diameter <2 µm, specific surface area ~750 m^{2}g^{-1}) were purchased from XG Sciences (Lansing, MI, USA) and used as received. Non-functionalized MWCNTs (NC7000 series, outer diameter ~9.5 nm, average length ~1.5 µm, specific surface area ~250–300 m^{2}g^{-1}) were purchased from Nanocyl S.A. (Sambreville, Belgium) and used as received. The GNP, MWCNT, and MDPE powders were mechanically mixed for 15 min. The mixed powders were used to create samples (1 cm × 1 cm × 0.15 cm) of MDPE/GNP at 2.5 wt%, 5 wt%, 10 wt%, and 15 wt%, of MDPE/MWCNT at 2.5 wt% and 5 wt%, and of MDPE loaded with 20 wt% of GNP/MWCNT hybrid filler in the ratio 3:1 (hereafter referred to as GNP_3MWCNT_1) by melting in oven at 125 °C while degassing.

The volumetric electrical conductivity of the specimens was determined by electrical impedance spectroscopy (EIS) using a Reference 600 Potentiostat/Galvanostat/ZRA instrument (Gamry Instruments, Warminster, PA, USA) in the frequency range 10 Hz–1 MHz. The specimens were placed in a custom-made Teflon cell and contacted by means of flat copper electrodes on the top and bottom sample surfaces (Figure 1). The cell was

closed in a Faraday cage (Gamry Instruments) to shield the measurements from undesired noise. Impedance data were fitted to an equivalent circuit model using the Gamry Echem Analyst software package. The electrical resistance values (R_s) obtained from the fitting procedure were converted to conductivities ($\sigma_v = 1/\rho_v$), where ρ_v is the volumetric resistivity evaluated according to the ASTM D257-07.

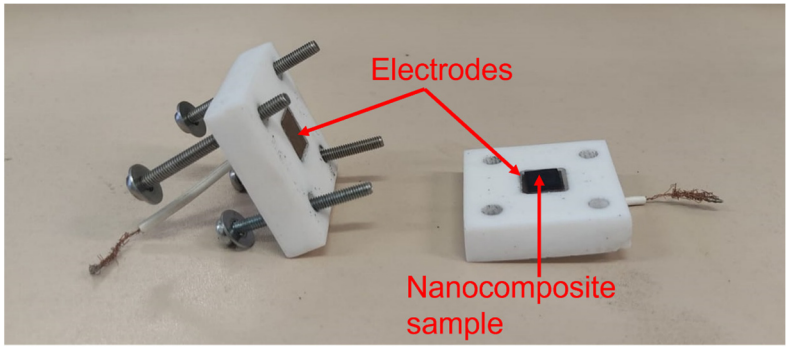

Figure 1. Set-up for electrical measurements: specimen (1 cm × 10 cm × 0.15 mm) placed in the custom-made Teflon cell and contacted by means of flat copper electrodes on the top and bottom surface.

Based on the electrical measurements, samples (5 cm × 5 cm × 0.5 cm) of MDPE/GNP at 5 wt%, 10 wt%, and 15 wt%, of MDPE/MWCNT at 5 wt%, and of MDPE/GNP_3MWCNT_1 were fabricated and subjected for an average time of 294 s to proton irradiation, at an energy of 64 MeV, current 1 nA, for a total dose of 50 Gy. The US Center for Diseases Control and Prevention on Acute Radiation Syndrome reports 50 Gy as the dose causing the fatal collapse of human cardiovascular and central nervous systems. The dose of 50 Gy is higher than the acceptable astronauts' exposure limits [39], and it was selected in this work to assess the shielding robustness of MDPE nanocomposites. The tests (Figure 2) were conducted at the Crocker Nuclear Laboratory of the University of California (Davis, CA, USA).

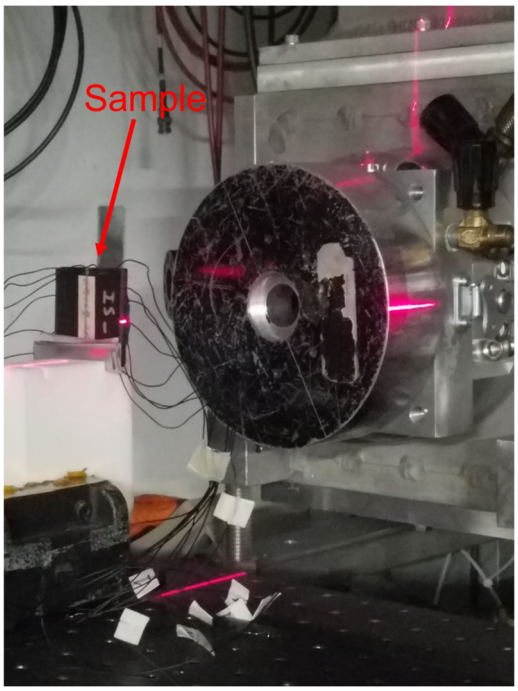

Figure 2. Sample of MDPE/GNP 5 wt% in proton irradiation line.

The Fourier transform infrared (FTIR) spectra of the nanocomposites before and after proton irradiation were studied using a Thermo-Scientific Nicolet Summit spectrometer equipped with an attenuated total reflection (ATR) accessory (ZnSe crystal). The ATR-FTIR spectra were acquired in the wavenumber range from 400 cm^{-1} to 4000 cm^{-1}, at a resolution of 4 cm^{-1} and auto scanning speed of 2 mm/s, keeping the air as a reference. The equation proposed by Zerbi et al. [40] is used to determine the degree of crystallinity (X_c) from FTIR spectra:

$$X_c = 100 - 100 \times \frac{1 - \left(\frac{I_a}{I_b}\right)/1.2333}{\left(1 + \frac{I_a}{I_b}\right)} \quad (1)$$

where I_a and I_b are the intensities of the bands at 730 cm^{-1} and 720 cm^{-1}, respectively. The constant 1.2333 corresponds to the relation of the intensities of these bands in the fully crystalline polyethylene spectrum [41].

Thermal analysis was performed using a double-furnace differential scanning calorimeter (DSC 8500, PerkinElmer, Waltham, MA, USA). Samples were sealed in aluminum pans with lids and measured in the temperature range from −45 °C to 150 °C with heating and cooling rates of 10 °C/min under nitrogen flow (20 cc/min). The degree of crystallinity was evaluated from the melting enthalpies (ΔH_m) determined as the area under the melting peak in the DSC thermograms, using the following equation:

$$X_c = 100 \times \Delta H_m / \Delta H_f (1 - w_f) \quad (2)$$

where ΔH_f is the latent heat of fusion of 100% crystalline polyethylene (288 J/g) [42] and w_f is the weight fraction of the nanoparticles.

The surface wettability of the nanocomposites was characterized by static contact angles (CA) measurements at the top surface using a DataPhysics OCA15Pro analyzer (DataPhysics Instruments, Filderstadt, Germany). The measurements were performed with the sessile drop method using degassed ultrapure water and diiodomethane as testing liquids. The determination of the contact angle values was performed according to the Young–Laplace fitting method using the DataPhysics SCA20 image analysis software. The values of the surface free energy (SFE) were determined with the Owens–Wendt method [43]:

$$\gamma(1 + \cos\theta) = 2\left[\left(\gamma_s^d \gamma_l^d\right)^{\frac{1}{2}} + \left(\gamma_s^p \gamma_l^p\right)^{\frac{1}{2}}\right] \quad (3)$$

where γ_s is the SFE of the solid that is analyzed, γ_l is the SFE of the measuring liquid, the apexes d and p indicate the dispersive and polar components, respectively, and θ is the contact angle between the solid and the testing liquid. The reported values of the CA and SFE are the average of ten measurements.

The morphology of the nanocomposites before and after proton irradiation was investigated using a VEGA II LSH scanning electron microscope (TESCAN, Brno, Czech Republic) with an accelerating voltage of 5 kV and a magnification of 500×. SEM images were acquired before and after proton exposure. The MountainsMap 7 software (Digital Surf, Besançon, France) was used to perform a 3D reconstruction of the specimen surface and the evaluation of surface roughness (R_a) from images acquired at different tilt angles (0° and 1°) [44]. The R_a was averaged over values determined on profiles extracted every 0.1 mm across the reconstructed 3D surface, typically 30 profiles for a surface area of 300 μm × 300 μm.

3. Results and Discussion

3.1. Electrical Properties

The volumetric electrical conductivity of MDPE/GNP at 2.5 wt%, 5 wt%, 10 wt%, and 15 wt%, of MDPE/MWCNT at 2.5 wt% and 5 wt%, and of MDPE/GNP_3MWCNT_1

at 20 wt% is given in Table 1. First, a significant enhancement of the electrical properties was observed, with the loading fraction increasing from 2.5 wt% to 5 wt% for both the MDPE/GNP and MDPE/MWCNT systems. Overall, the MDPE/MWCNT system shows higher electrical conductivities than the MDPE/GNP system at all mass concentrations due to the presence of the MWCNTs with their high aspect ratio. In addition, the difference between the electrical conductivity of the MDPE/GNP at 5 wt%, 10 wt%, and 15 wt% is negligible, meaning that further increasing the nanofiller concentration has a minimal effect. As regards the MDPE/GNP_3MWCNT_1 20 wt% nanocomposite, it shows the highest electrical conductivity among the investigated systems due to the synergistic effect of the GNPs and CNTs nanoparticles: the high aspect ratio of MWCNTs is responsible for the high electrical conductivity and for preventing the restacking of the GNPs, while the GNPs inhibit the aggregation of the MWCNTs, creating an interconnected hybrid architecture [45]. In order to explore the potential applications of carbon-based multifunctional nanocomposites with high electrical conductivity in space radiation environments and the effects of different nanofiller loadings on the radiation sensitivity of these materials, samples (5 cm × 5 cm × 5 cm) of MDPE/GNP at 5 wt%, 10 wt%, and 15 wt%, of MDPE/MWCNT at 5 wt%, and of MDPE/GNP_3MWCNT_1 20 wt% were subjected to proton radiation and their properties were investigated in terms of chemical structure, thermal behavior, wettability, and morphology.

Table 1. Electrical conductivity of MDPE/GNP and MDPE/MWCNT samples at different filler concentrations, and MDPE/GNP_3MWCNT_1 20 wt% nanocomposite.

Sample	σ_v (S/mm)
MDPE/GNP 2.5 wt%	$1.81 \times 10^{-14} \pm 5.1 \times 10^{-15}$
MDPE/GNP 5 wt%	$2.10 \times 10^{-13} \pm 1.4 \times 10^{-14}$
MDPE/GNP 10 wt%	$1.53 \times 10^{-12} \pm 3.9 \times 10^{-14}$
MDPE/GNP 15 wt%	$7.63 \times 10^{-12} \pm 8.0 \times 10^{-14}$
MDPE/MWCNT 2.5 wt%	$6.93 \times 10^{-9} \pm 4.6 \times 10^{-10}$
MDPE/MWCNT 5 wt%	$2.26 \times 10^{-7} \pm 1.1 \times 10^{-8}$
MDPE/GNP_3MWCNT_1 20 wt%	$2.86 \times 10^{-7} \pm 1.0 \times 10^{-8}$

3.2. FTIR Analysis

Samples (5 cm × 5 cm × 5 cm) of MDPE/GNP at 5 wt%, 10 wt%, and 15 wt%, of MDPE/MWCNT at 5 wt%, and of MDPE/GNP_3MWCNT_1 at 20 wt% were subjected to proton radiation and the chemical changes induced by the exposure were identified by ATR-FTIR, obtaining the spectra (raw data) reported in Figures S1 and S2. The main absorption peaks of polyethylene are given in Table 2, in agreement with the literature [46].

Table 2. Main absorption bands of polyethylene in the IR region and their assignments.

Band (cm^{-1})	Assignment
2914	CH_2 asymmetric deformation
2847	CH_2 symmetric deformation
1472, 1462	Bending deformation
1376	CH_2 symmetric deformation
729, 718	Rocking deformation

The addition of GNP and MWCNT nanofillers did not significantly modify the shape of the vibrational spectra of the MDPE matrix. However, two main effects induced by irradiation in atmosphere are observed: oxidative degradation and crystallinity changes. Figures 3 and 4 show ATR-FTIR spectra of the nanocomposites before and after proton irradiation in the 750–700 cm^{-1} region, where the doublet at 718–729 cm^{-1} was analyzed. Table 3 illustrates the X_c of the nanocomposites before and after proton irradiation, cal-

culated using the equation proposed by Zerbi et al. [40]. The intensities of the bands at 729 cm^{-1} and 718 cm^{-1} and their ratios are reported in Table S1.

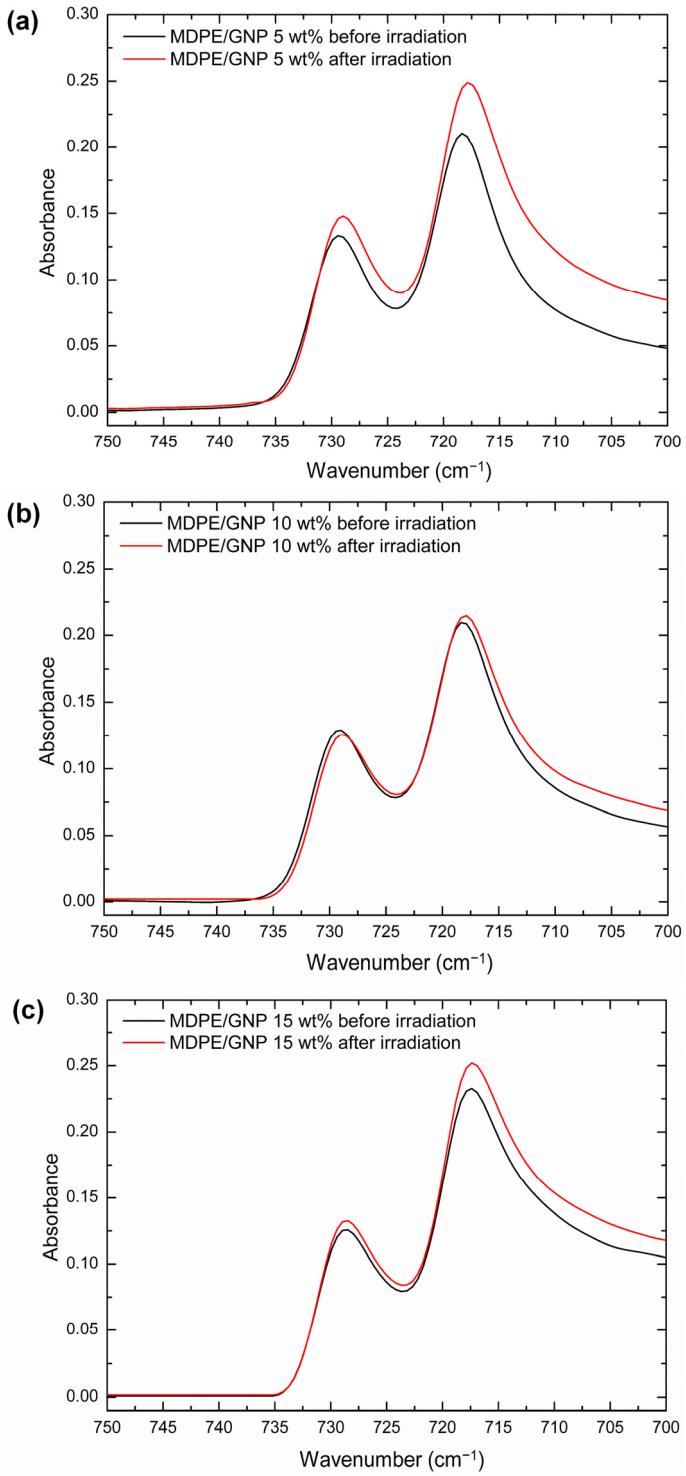

Figure 3. ATR-FTIR spectra of (**a**) MDPE/GNP 5 wt%, (**b**) MDPE/GNP 10 wt%, (**c**) MDPE/GNP 15 wt% nanocomposites before and after proton irradiation in the 750–700 cm^{-1} region.

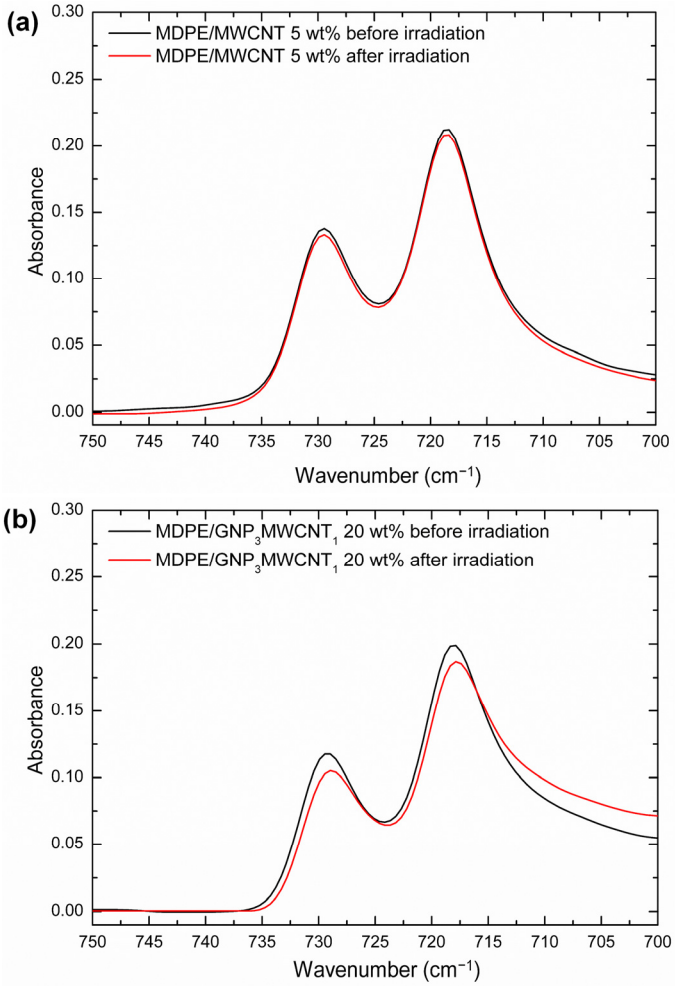

Figure 4. ATR-FTIR spectra of (**a**) MDPE/MWCNT 5 wt% and (**b**) MDPE/GNP_3MWCNT_1 nanocomposites before and after proton irradiation in the 750–700 cm^{-1} region.

Table 3. Degree of crystallinity (X_c) and relative percentage variation ($\Delta X_c/X_c$) calculated from FTIR spectra of MDPE/GNP and MDPE/MWCNT nanocomposites at different filler concentrations and MDPE/GNP_3MWCNT_1 20 wt% sample before and after proton irradiation. Standard deviation of data is below 2%.

Sample	X_c (%) (by FTIR)		$\Delta X_c/X_c$ (%)
	Non-Irradiated	Irradiated	
MDPE/GNP 5 wt%	70.0	67.5	−3.6
MDPE/GNP 10 wt%	69.1	66.9	−3.2
MDPE/GNP 15 wt%	63.6	62.6	−1.6
MDPE/MWCNT 5 wt%	71.4	70.6	−1.1
MDPE/GNP_3MWCNT_1 20 wt%	67.4	65.1	−3.4

First, a slight decrease in X_c is observed as the GNP content increases, which can be attributed to the tendency of GNP to hinder the molecular mobility of the polymer matrix at relatively high concentrations (above 3–5 wt%) [47,48], thus limiting the growth of polyethylene crystallites [48]. The MDPE/MWCNT 5 wt% samples show slightly higher X_c values than the MDPE/GNP 5 wt% nanocomposites since the GNP filler imposes more constraints around the polymer chains, inducing a greater fraction of polymer chains to be trapped in the graphene network [49]. All nanocomposites show a decrease in X_c after exposure to proton radiation; however, this effect is negligible for the MDPE/MWCNT

5 wt% sample. Furthermore, as the filler content increases, the relative percentage variations in X_c (indicated as $\Delta X_c/X_c$) decrease, confirming an increasing shielding effect with increasing filler content. Overall, the decrease of X_c after irradiation can be explained by branching and cross-linking phenomena, in accordance with the current literature [50–53]. In the case of irradiation of polymeric materials, macro radicals will be generated both in the amorphous and crystalline phases. These radicals can then react with molecular or atomic oxygen leading to the formation of ketones, aldehydes, alcohols, and carboxylic acids. The selected GNP nanoparticles have nitrogen and oxygen atoms attached to the graphene sheets that are likely cleaved when irradiated [54,55]. The generated free radicals can react with polyethylene, leading to the formation of cross-linked bonds in the side chains of the polymer matrix. In this way, the increase of short-chain branching density decreases the lamellar thickness of the crystal structure, consequently reducing the X_c of irradiated samples [53,56].

3.3. Thermal Analysis by Differential Scanning Calorimetry

The thermal behavior of the nanocomposites was analyzed by DSC before and after proton irradiation. Thermograms of heating and cooling of the samples are reported in Figures 5 and 6, respectively. Results from thermal analysis are summarized in Tables 4 and 5. As the samples were irradiated in a solid state, the first heating cycle was used to investigate changes in crystallinity induced by radiation, and the results were compared with those obtained by FTIR.

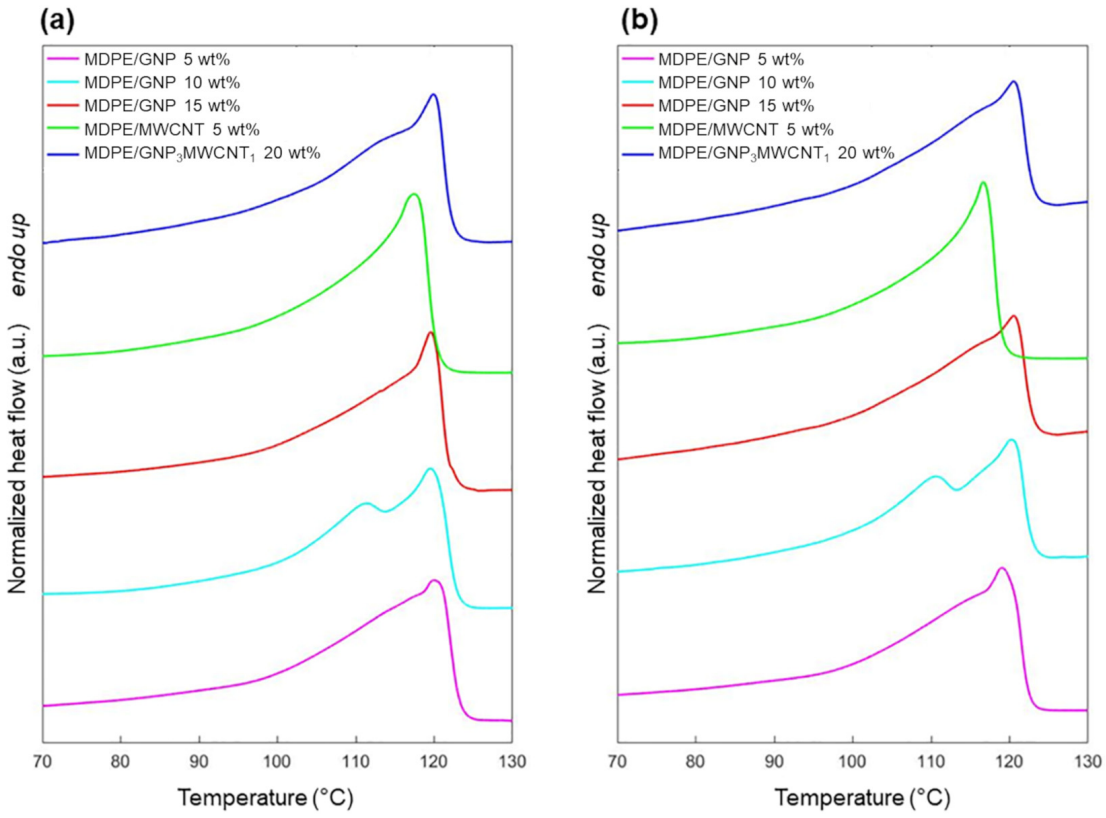

Figure 5. DSC thermograms upon heating for MDPE/GNP 5 wt%, MDPE/GNP 10 wt%, MDPE/GNP 15 wt%, MDPE/MWCNT 5 wt% and MDPE/GNP_3MWCNT_1 20 wt% nanocomposites (**a**) before and (**b**) after proton irradiation. Heating rate: 10 °C/min. Heat flow is normalized by the sample weight. Data are offset for clarity.

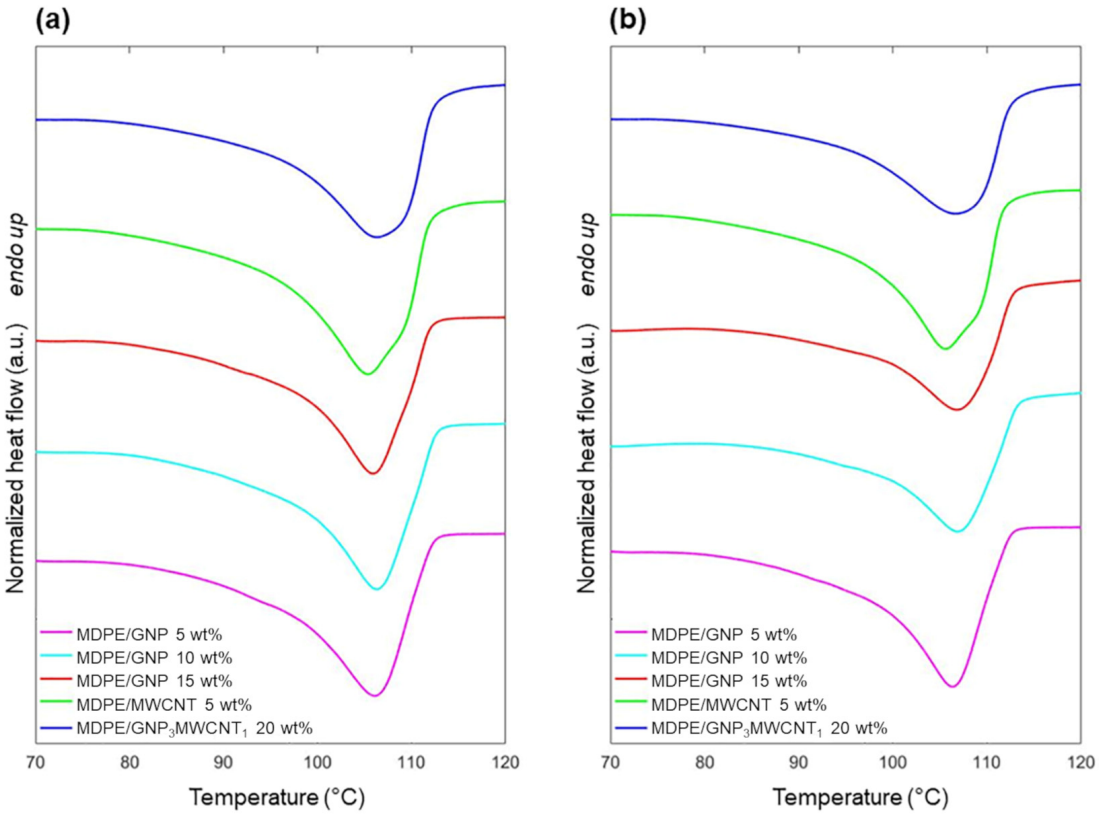

Figure 6. DSC thermograms upon cooling for MDPE/GNP 5 wt%, MDPE/GNP 10 wt%, MDPE/GNP 15 wt%, MDPE/MWCNT 5 wt% and MDPE/GNP_3MWCNT_1 20 wt% nanocomposites (**a**) before and (**b**) after proton irradiation. Heating rate: 10 °C/min. Heat flow is normalized by the sample weight. Data are offset for clarity.

Table 4. DSC results for MDPE/GNP and MDPE/MWCNT samples at different filler concentrations, and for the MDPE/GNP_3MWCNT_1 20 wt% nanocomposite before and after proton irradiation. Standard deviation of data are below 2%.

Non-Irradiated	T_m (°C)	ΔH_m (J/g)	T_c (°C)	ΔH_c (J/g)
MDPE/GNP 5 wt%	120.0	147.3	106.1	125.8
MDPE/GNP 10 wt%	119.5	137.2	106.3	121.4
MDPE/GNP 15 wt%	119.6	120.9	106.0	115.3
MDPE/MWCNT 5 wt%	117.5	152.4	105.4	141.0
MDPE/GNP_3MWCNT_1 20 wt%	120.0	127.9	106.4	121.6
Irradiated	**T_m (°C)**	**ΔH_m (J/g)**	**T_c (°C)**	**ΔH_c (J/g)**
MDPE/GNP 5 wt%	119.0	137.1	106.4	119.8
MDPE/GNP 10 wt%	120.2	128.7	107.0	110.2
MDPE/GNP 15 wt%	120.1	114.7	107.0	109.0
MDPE/MWCNT 5 wt%	116.6	148.5	105.6	136.7
MDPE/GNP_3MWCNT_1 20 wt%	120.5	123.9	106.8	113.5

Table 5. Degree of crystallinity (X_c) and relative percentage variation ($\Delta X_c/X_c$) calculated by DSC of MDPE/GNP and MDPE/MWCNT nanocomposites at different filler concentrations and MDPE/GNP_3MWCNT_1 20 wt% sample before and after proton irradiation. Standard deviation of data is below 2%.

Sample	X_c (%) (by DSC)		$\Delta X_c / X_c$ (%)
	Non-Irradiated	Irradiated	
MDPE/GNP 5 wt%	53.8	50.1	−6.9
MDPE/GNP 10 wt%	52.9	49.7	−6.2
MDPE/GNP 15 wt%	49.4	46.9	−5.2
MDPE/MWCNT 5 wt%	55.7	54.3	−2.6
MDPE/GNP_3MWCNT_1 20 wt%	55.5	53.8	−3.1

As shown in Table 4, only small differences in the values of the melting (T_m) and crystallization (T_c) temperatures are observed among the different nanocomposites and after the radiation process. Results regarding the degree of crystallinity calculated by DSC (Table 5) confirm the same trend showed by ATR-FTIR analysis. In fact, also, in this case, comparing the X_c values before and after proton exposure, a decrease in crystallinity caused by the irradiation can be observed, and this is more evident in the presence of the GNP filler. Further, the presence of a shoulder in the nanocomposites containing GNP was observed (Figure 5), and it can be ascribed to the melting of imperfect crystals. This phenomenon can be related to the more constraints imposed by the GNP filler on the polymer matrix [49], favoring the formation of imperfect crystalline lamellae. For the samples containing GNPs, the decrease of ΔH_c upon irradiation confirms that the formation of cross-links and chain branches hinders the polymer chain's mobility and chain reorganization during the crystallization process, leading to the formation of imperfect and thinner lamellae [57]. As anticipated in the ATR-FTIR analysis, the values of X_c and ΔH_c of the MDPE/MWCNT 5 wt% nanocomposite are less affected by proton irradiation. Although the trend in the degree of crystallinity is the same, X_c values determined by FTIR are higher for all samples. This has already been reported in the literature and can be mainly ascribed to some limitations of the DSC technique. In fact, the crystallinity of the polymer is temperature dependent, and the estimated crystallinity determined by DSC at the melting temperature will differ from the value at ambient temperature [48,58]. Moreover, the differential nature and overlap of multiple thermal events (chain relaxation, melting of different crystal forms) can affect the values of X_c determined by DSC. Nevertheless, the DSC technique allows for detecting bulk features, whereas ATR-FTIR mainly reveals the surface characteristics of the material. Overall, these two techniques should be considered complementary to better understand the behavior of the nanocomposites. In fact, it is possible that irradiation induced chain-branching and cross-linking on top of the irradiated surface, while chain scission is predominant in the bulk of the sample.

3.4. Contact Angle Measurements

The wetting behavior before and after proton irradiation was investigated by static contact angle measurements in sessile drop configuration. The water contact angle (WCA) and SFE values are given in Table 6, showing an alteration of the WCA and SFE of irradiated samples compared with the non-irradiated ones. The analysis revealed the hydrophobicity of the non-irradiated nanocomposites, which are characterized by WCA values above 105°. The WCA strongly increases with nanofiller content, reaching 115.7° ± 2.5° for the hybrid nanocomposite. After proton exposure, the WCA of all nanocomposites decreased, with the largest variation in surface wettability observed in the MDPE/MWCNT 5 wt% nanocomposite (11.1%). The surface hydrophobicity of the PE/GNP nanocomposites was reduced in proportion to the GNP content, with the smallest WCA decrease (3.2%) for the MDPE/GNP 5 wt% surface and the largest (8.4%) for the MDPE/GNP 15 wt% surface. It is known that the WCA of a polymer surface depends on chemical functional groups and

asperities: it decreases with increasing surface energy and surface smoothness [59]. Hence, to further investigate the decrease of the WCA values occurring upon irradiation, a surface-free energy analysis following the Owens–Wendt method [43] was carried out with two different testing liquids (water and diiodomethane). As shown in Table 6, the SFE decreases at increasing nanofiller content in non-irradiated samples. The dispersive component (γ^d), which is due to the dispersive interactions among non-polar molecules, is predominant over the polar one (γ^p) for all investigated samples. After proton exposure, the SFE and its dispersive component show a marked increase in the nanocomposite samples. On the contrary, the polar component decreases in GNP-loaded nanocomposites, and increases in the MDPE/MWCNT 5 wt% nanocomposite. The decrease of surface hydrophobicity upon irradiation is in agreement with reports in the literature [21,22,60]. It can be ascribed to an oxidation phenomenon in the MDPE/MWCNT 5 wt% nanocomposite (as revealed by the increase of γ^p) and to the formation of nonpolar chain branches in GNP-loaded nanocomposites (as revealed by the increase of γ^d). In fact, it was demonstrated that the oxygen content in proton-irradiated MWCNTs is higher than in non-irradiated ones [61]. This behavior has not been observed for the MDPE/GNP_3MWCNT_1 20 wt% samples, and this can be explained by the predominant presence of GNP (GNP/MWCNT ratio of 3:1), which may plausibly mitigate this phenomenon. In addition, the morphological analysis of the nanocomposite surface reported below shows the improved surface smoothness of irradiated samples, which also contributes to the decrease of the WCA [59].

Table 6. Water contact angles (WCA) and surface free energies (SFE) with dispersive (γ^d) and polar (γ^p) components of MDPE/GNP 5 wt%, MDPE/GNP 10 wt%, MDPE/GNP 15 wt%, PE/MWCNT 5 wt% and MDPE/GNP_3MWCNT_1 20 wt% before and after proton irradiation.

Non-Irradiated	**WCA (°)**	**SFE (mJ/m^2)**	**γ^p**	**γ^d**
MDPE/GNP 5 wt%	110.1 ± 1.8	36.25	0.19	36.06
MDPE/GNP 10 wt%	112.5 ± 1.1	31.92	0.16	31.76
MDPE/GNP 15 wt%	113.1 ± 1.7	31.33	0.17	31.16
MDPE/MWCNT 5 wt%	105.4 ± 1.8	31.03	0.05	30.98
MDPE/GNP_3MWCNT_1 20 wt%	115.7 ± 2.5	29.02	0.24	28.78
Irradiated	**WCA (°)**	**SFE (mJ/m^2)**	**γ^p**	**γ^d**
MDPE/GNP 5 wt%	106.6 ± 1.6	36.44	0.03	36.42
MDPE/GNP 10 wt%	104.3 ± 2.0	32.97	0.05	32.92
MDPE/GNP 15 wt%	103.6 ± 5.3	35.81	0.02	35.80
MDPE/MWCNT 5 wt%	93.7 ± 1.1	36.43	0.98	35.45
MDPE/GNP_3MWCNT_1 20 wt%	103.0 ± 2.8	34.17	0.07	34.10

3.5. Morphological Analysis

The surface morphology of the nanocomposites before and after proton irradiation was investigated by SEM (Figures 7 and 8). The images reveal the erosive effect of radiation that is more evident at high nanofiller loadings, with the surfaces of the nanocomposites appearing smoother after exposure.

Due to the formation of entanglements at high nanofiller contents, we find an increasing number of surface asperities with increasing filler concentrations. In particular, we observe a high number of small peaks on the surface of MDPE/GNP specimens. By contrast, the surface morphology of the MDPE/MWCNT 5 wt% and MDPE/GNP_3MWCNT_1 20 wt% samples is characterized by the presence of large peaks. The reason is attributed to the large aggregates formed due to the weak interaction of the pristine MWCNTs with the MDPE matrix and to the van der Waals forces acting among the MWCNT nanoparticles. A 3D reconstruction of the surface profiles was performed to quantify the effect of the radiation exposure at the top surface of the nanocomposite samples. 3D images were obtained with the Mountains Map software, starting from two SEM images acquired at two different tilt angles (0° and 1°). Results of the 3D surface reconstruction are reported in Figures 9 and 10.

A decrease in the height of surface peaks in irradiated nanocomposites is clearly visible on the color-scaled SEM images, which corresponds to an increased surface smoothness.

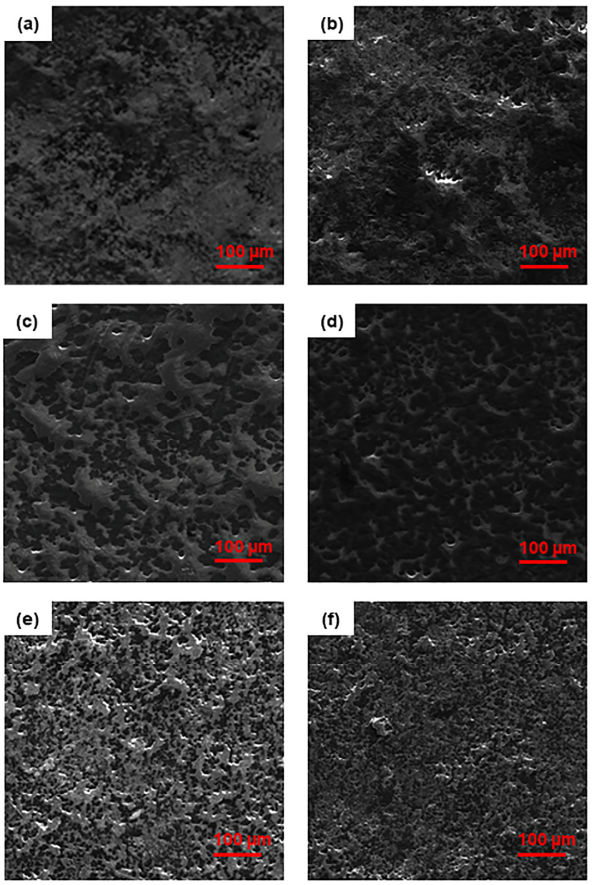

Figure 7. SEM images of non-irradiated (**left**) and irradiated (**right**) samples of (**a**,**b**) MDPE/GNP 5 wt%, (**c**,**d**) MDPE/GNP 10 wt%, (**e**,**f**) MDPE/GNP 15 wt% nanocomposites.

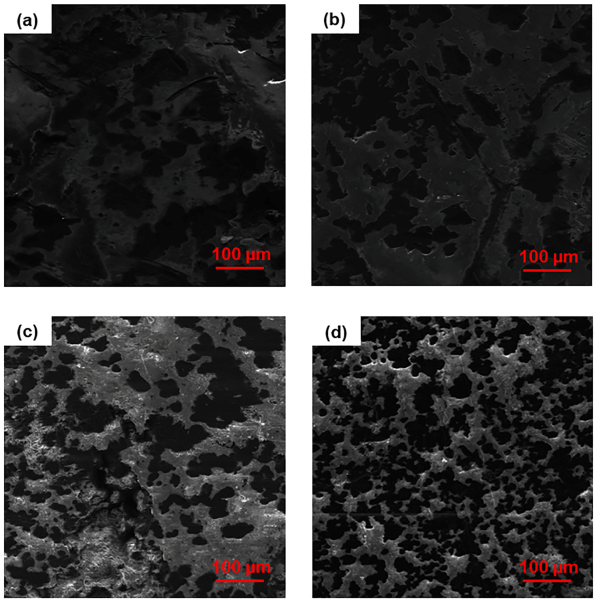

Figure 8. SEM images of non-irradiated (**left**) and irradiated (**right**) samples of (**a**,**b**) MDPE/MWCNT 5 wt% and (**c**,**d**) MDPE/GNP_3MWCNT_1 20 wt% nanocomposites.

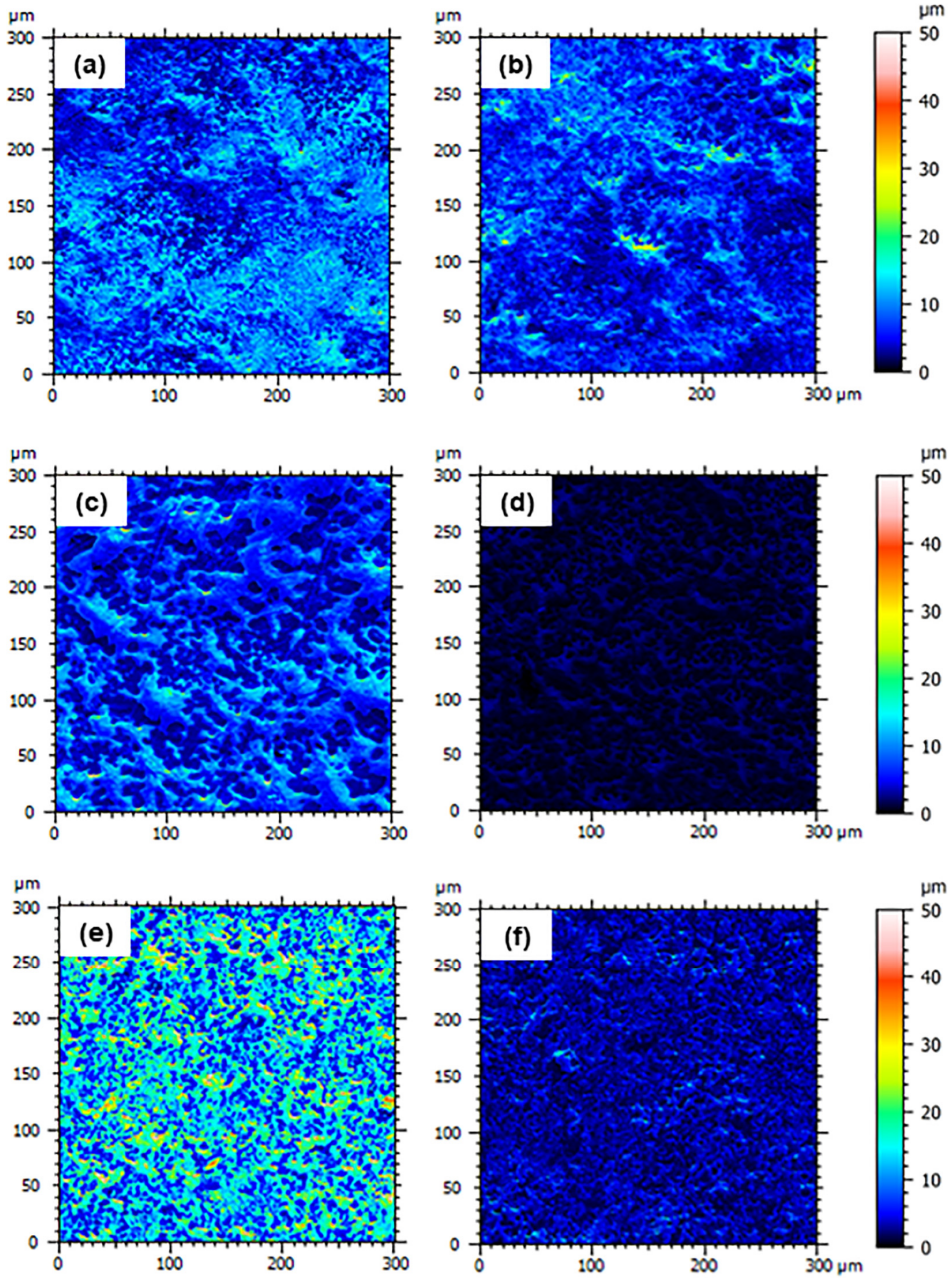

Figure 9. 3D surface reconstruction through SEM image processing of non-irradiated (**left**) and irradiated (**right**) samples of (**a**,**b**) MDPE/GNP 5 wt%, (**c**,**d**) MDPE/GNP 10 wt%, (**e**,**f**) MDPE/GNP 15 wt% nanocomposites.

Table 7 presents the R_a values of the nanocomposites before and after proton irradiation. Despite the different nanofiller concentrations, the MDPE/GNP_3MWCNT_1 20 wt% and MDPE/GNP 15 wt% non-irradiated nanocomposites show similar values of the R_a. This result is explained by the presence of both GNP and MWCNT nanofillers in the hybrid system, where the graphene nanoplatelets prevent the aggregation of nanotubes by physically hindering the process due to their large surface area [45]. All nanocomposites show a significant decrease of R_a upon exposure to proton radiation, with the largest variation observed in the MDPE/GNP 15 wt% (76.5%). This result confirms the cleavage effect of irradiation on the edges of the GNPs and subsequent surface erosion.

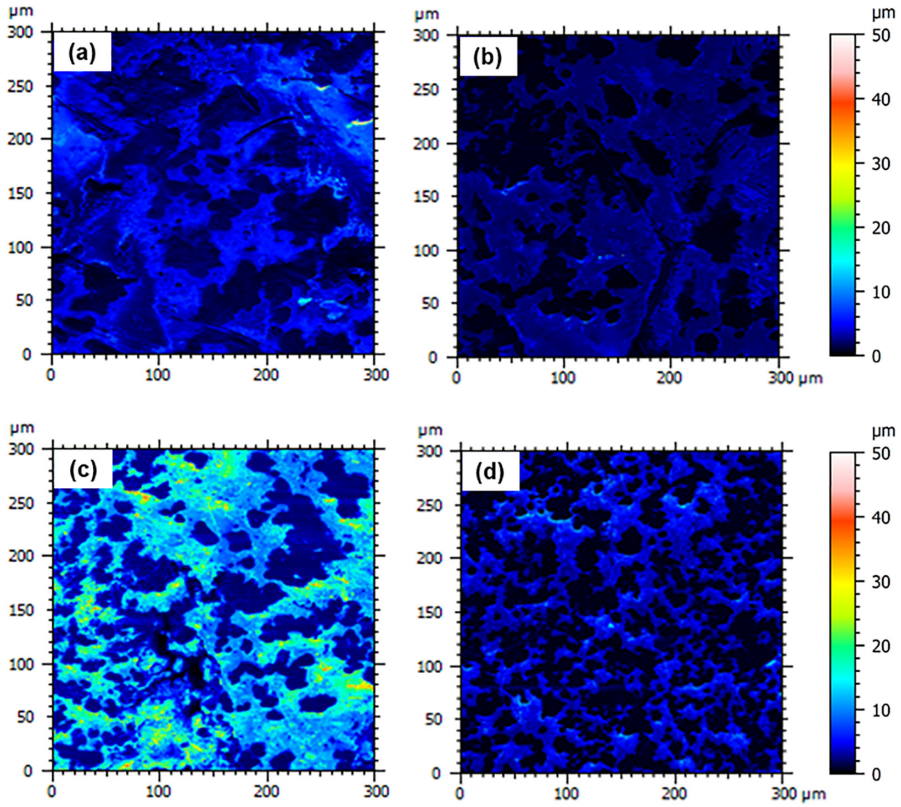

Figure 10. 3D surface reconstruction through SEM image processing of non-irradiated (**left**) and irradiated (**right**) samples of (**a**,**b**) MDPE/MWCNT 5 wt% and (**c**,**d**) MDPE/GNP_3MWCNT_1 20 wt% nanocomposites.

Table 7. Surface roughness and relative percentage variation ($\Delta R_a/R_a$) of MDPE/GNP 5 wt%, MDPE/GNP 10 wt%, MDPE/GNP 15 wt%, MDPE/MWCNT 5 wt% and MDPE/GNP_3MWCNT_1 20 wt% nanocomposites before and after proton irradiation.

Sample	R_a (µm)		$\Delta R_a/R_a$ (%)
	Non-Irradiated	Irradiated	
MDPE/GNP 5 wt%	3.6 ± 0.5	2.6 ± 0.4	−27.8
MDPE/GNP 10 wt%	6.7 ± 1.6	2.2 ± 0.3	−67.2
MDPE/GNP 15 wt%	5.1 ± 0.6	1.2 ± 0.2	−76.5
MDPE/MWCNT 5 wt%	3.6 ± 0.6	2.4 ± 0.3	−33.3
MDPE/GNP_3MWCNT_1 20 wt%	5.1 ± 0.8	2.1 ± 0.3	−58.8

4. Conclusions

In this work, the sensitivity to proton radiation of nanocomposites made of medium-density polyethylene (MDPE) loaded with different amounts of GNP and MWCNT nanofillers was investigated. Different techniques were used to study the nanocomposite's response in terms of chemical structure, thermal behavior, wettability, and morphology. Results regarding the degree of crystallinity evaluated by FTIR and DSC unveiled a higher decrease of crystallinity after proton irradiation in the nanocomposites filled with GNP due to the branching and cross-linking mechanisms induced by the radiation. The MDPE/MWCNT 5 wt% nanocomposite showed the highest degree of crystallinity, with unnoteworthy changes after irradiation. The DSC analysis showed the thermal stability of the investigated nanocomposites in response to radiation, with T_m and T_c that remained unaltered. Despite a decrease in the WCA values of all nanocomposites after proton exposure, all samples maintained a hydrophobic surface and, therefore, a low tendency to adsorb water vapor

from the environment. Lastly, a 3D reconstruction of the surface profiles was performed to quantify the effect of the radiation exposure at the top surface of the nanocomposite samples, revealing an increased surface smoothness after irradiation. Nevertheless, this effect is less marked in the MDPE/GNP 5 wt% and MDPE/MWCNT 5 wt% nanocomposites.

Overall, the results of this work show that the MDPE/MWCNT 5 wt% material is the best MDPE/nanocarbon system for use in radiation shielding applications due to the negligible changes observed in the physico-chemical properties after proton irradiation.

Supplementary Materials: The following supporting information can be downloaded at: https://www.mdpi.com/article/10.3390/nano13071288/s1, Figure S1: ATR-FTIR spectra (raw data) of (**a**) MDPE /GNP 5 wt%, (**b**) MDPE /GNP 10 wt% and (**c**) MDPE/GNP 15 wt% nanocomposites before and after proton irradiation. Data are offset for clarity; Figure S2: ATR-FTIR spectra (raw data) of (**a**) MDPE/MWCNT 5 wt% and (**b**) MDPE/GNP_3MWCNT_1 20 wt% nanocomposites before and after proton irradiation. Data are offset for clarity; Table S1: ATR-FTIR data of non-irradiated and irradiated nanocomposites: intensity of the band at 729 cm^{-1} (I_a) and 718 cm^{-1} (I_b) and their ratio (I_a/I_b).

Author Contributions: Conceptualization, S.L.; methodology, M.G.S. and S.L.; validation, M.G.S. and S.L.; formal analysis, F.Z., E.T. and S.R.; investigation, F.Z., E.T., S.R. and V.L.S.; writing—original draft preparation, F.Z.; writing—review and editing, E.T., M.G.S. and S.L.; supervision, M.G.S., S.L. and V.L.S.; funding acquisition, S.L and V.L.S. All authors have read and agreed to the published version of the manuscript.

Funding: This research was funded by Sapienza University of Rome (grant number RM120172B73FC9DC) and by the NASA Solar System Exploration Research Virtual Institute (agreement #NNA17BF68A).

Institutional Review Board Statement: Not applicable.

Informed Consent Statement: Not applicable.

Data Availability Statement: Data are contained within the article or Supplementary Material.

Conflicts of Interest: The authors declare no conflict of interest.

References

1. Teo, A.J.T.; Mishra, A.; Park, I.; Kim, Y.-J.; Park, W.-T.; Yoon, Y.-J. Polymeric Biomaterials for Medical Implants and Devices. *ACS Biomater. Sci. Eng.* **2016**, *2*, 454–472. [CrossRef] [PubMed]
2. Auras, R.; Harte, B.; Selke, S. An Overview of Polylactides as Packaging Materials. *Macromol. Biosci.* **2004**, *4*, 835–864. [CrossRef] [PubMed]
3. Durante, M. Space radiation protection: Destination Mars. *Life Sci. Space Res.* **2014**, *1*, 2–9. [CrossRef]
4. Zaccardi, F.; Toto, E.; Santonicola, M.G.; Laurenzi, S. 3D printing of radiation shielding polyethylene composites filled with Martian regolith simulant using fused filament fabrication. *Acta Astronaut.* **2022**, *190*, 1–13. [CrossRef]
5. Thibeault, S.A.; Kang, J.H.; Sauti, G.; Park, C.; Fay, C.C.; King, G.C. Nanomaterials for radiation shielding. *MRS Bull.* **2015**, *40*, 836–841. [CrossRef]
6. Laurenzi, S.; de Zanet, G.; Santonicola, M.G. Numerical investigation of radiation shielding properties of polyethylene-based nanocomposite materials in different space environments. *Acta Astronaut.* **2020**, *170*, 530–538. [CrossRef]
7. Singh, B.P.; Prabha; Saini, P.; Gupta, T.; Garg, P.; Kumar, G.; Pande, I.; Pande, S.; Seth, R.K.; Dhawan, S.K.; et al. Designing of multiwalled carbon nanotubes reinforced low density polyethylene nanocomposites for suppression of electromagnetic radiation. *J. Nanopart. Res.* **2011**, *13*, 7065–7074. [CrossRef]
8. Xie, R.; Wang, J.; Yang, Y.; Jiang, K.; Li, Q.; Fan, S. Aligned carbon nanotube coating on polyethylene surface formed by microwave radiation. *Compos. Sci. Technol.* **2011**, *72*, 85–90. [CrossRef]
9. Liao, Q.; Liu, Z.; Liu, W.; Deng, C.; Yang, N. Extremely High Thermal Conductivity of Aligned Carbon Nanotube-Polyethylene Composites. *Sci. Rep.* **2015**, *5*, 16543. [CrossRef]
10. Kanagaraj, S.; Varanda, F.R.; Zhil'tsova, T.V.; Oliveira, M.S.A.; Simões, J.A.O. Mechanical properties of high density polyethylene/carbon nanotube composites. *Compos. Sci. Technol.* **2007**, *67*, 3071–3077. [CrossRef]
11. Ruoff, R.S.; Lorents, D.C. Mechanical and thermal properties of carbon nanotubes. *Carbon* **1995**, *33*, 925–930. [CrossRef]
12. Maffucci, A.; Miano, G. Electrical Properties of Graphene for Interconnect Applications. *Appl. Sci.* **2014**, *4*, 305–317. [CrossRef]
13. Bernholc, J.; Brenner, D.; Buongiorno Nardelli, M.; Meunier, V.; Roland, C. Mechanical and electrical properties of nanotubes. *Annu. Rev. Mater. Res.* **2002**, *32*, 347–375. [CrossRef]
14. Abdul-Kader, A.; Turos, A.; Jagielski, J.; Nowicki, L.; Ratajczak, R.; Stonert, A.; Al-Ma'adeed, M.A. Hydrogen release in UHMWPE upon He-ion bombardment. *Vacuum* **2005**, *78*, 281–284. [CrossRef]

15. Oral, E.; Muratoglu, O.K. Radiation cross-linking in ultra-high molecular weight polyethylene for orthopaedic applications. *Nucl. Instrum. Methods Phys. Res. Sect. B* **2007**, *265*, 18–22. [CrossRef]
16. Rui, E.; Yang, J.; Li, X.; Ma, G. Effect of proton irradiation on mechanical properties of low-density polyethylene/multiwalled carbon nanotubes composites. *Polym. Compos.* **2015**, *36*, 278–286. [CrossRef]
17. Saif, M.J.; Naveed, M.; Asif, H.M.; Akhtar, R. Irradiation applications for polymer nano-composites: A state-of-the-art review. *J. Ind. Eng. Chem.* **2018**, *60*, 218–236. [CrossRef]
18. Toto, E.; Laurenzi, S.; Santonicola, M.G. Recent Trends in Graphene/Polymer Nanocomposites for Sensing Devices: Synthesis and Applications in Environmental and Human Health Monitoring. *Polymers* **2022**, *14*, 1030. [CrossRef]
19. Clausi, M.; Toto, E.; Botti, S.; Laurenzi, S.; La Saponara, V.; Santonicola, M.G. Direct effects of UV irradiation on graphene-based nanocomposite films revealed by electrical resistance tomography. *Compos. Sci. Technol.* **2019**, *183*, 107823. [CrossRef]
20. Santonicola, M.; Toto, E.; Palombi, M.; Paris, C.; Laurenzi, S. Experimental study of solar radiation effects on carbon nanocomposite sensors in simulated space environment. In Proceedings of the International Astronautical Congress, IAC, Bremen, Germany, 1–5 October 2018.
21. Toto, E.; Botti, S.; Laurenzi, S.; Santonicola, M.G. UV-induced modification of PEDOT: PSS-based nanocomposite films investigated by Raman microscopy mapping. *Appl. Surf. Sci.* **2020**, *513*, 145839. [CrossRef]
22. Toto, E.; Palombi, M.; Laurenzi, S.; Santonicola, M.G. Functional nanocomposites with graphene-DNA hybrid fillers: Synthesis and surface properties under UV irradiation. *Ceram. Int.* **2019**, *45*, 9631–9637. [CrossRef]
23. Boul, P.J.; Turner, K.; Li, J.; Pulikkathara, M.X.; Dwivedi, R.C.; Sosa, E.D.; Lu, Y.; Kuznetsov, O.V.; Moloney, P.; Wilkins, R.; et al. Single Wall Carbon Nanotube Response to Proton Radiation. *J. Phys. Chem. C* **2009**, *113*, 14467–14473. [CrossRef]
24. Cui, F.Z.; Chen, Z.J.; Ma, J.; Xia, G.R.; Zhai, Y. Atomistic simulation of radiation damage to carbon nanotube. *Phys. Lett. A* **2002**, *295*, 55–59. [CrossRef]
25. Salonen, E.; Krasheninnikov, A.V.; Nordlund, K. Ion-irradiation-induced defects in bundles of carbon nanotubes. *Nucl. Instrum. Methods Phys. Res. Sect. B* **2002**, *193*, 603–608. [CrossRef]
26. Kis, A.; Csányi, G.; Salvetat, J.-P.; Lee, T.-N.; Couteau, E.; Kulik, A.J.; Benoit, W.; Brugger, J.; Forró, L. Reinforcement of single-walled carbon nanotube bundles by intertube bridging. *Nat. Mater.* **2004**, *3*, 153–157. [CrossRef] [PubMed]
27. Chen, S.; Nambiar, S.; Li, Z.; Osei, E.; Darko, J.; Zheng, W.; Sun, Z.; Liu, P.; Yeow, J.T.W. Bismuth oxide-based nanocomposite for high-energy electron radiation shielding. *J. Mater. Sci.* **2019**, *54*, 3023–3034. [CrossRef]
28. Nielsen, K.L.C.; Hill, D.J.T.; Watson, K.A.; Connell, J.W.; Ikeda, S.; Kudo, H.; Whittaker, A.K. The radiation degradation of a nanotube–polyimide nanocomposite. *Polym. Degrad. Stab.* **2008**, *93*, 169–175. [CrossRef]
29. Li, Z.; Nambiar, S.; Zheng, W.; Yeow, J.T.W. PDMS/single-walled carbon nanotube composite for proton radiation shielding in space applications. *Mater. Lett.* **2013**, *108*, 79–83. [CrossRef]
30. Najafi, E.; Shin, K. Radiation resistant polymer–carbon nanotube nanocomposite thin films. *Colloids Surf. A Physicochem. Eng. Asp.* **2005**, *257–258*, 333–337. [CrossRef]
31. Wilkins, R.; Pulikkathara, M.X.; Khabashesku, V.N.; Barrera, E.V.; Vaidyanathan, R.K.; Thibeault, S.A. Ground-Based Space Radiation Effects Studies on Single-Walled Carbon Nanotube Materials. *MRS Online Proc. Lib.* **2004**, *851*, 380–391. [CrossRef]
32. Lee, S.; Seo, J.; Hong, J.; Park, S.H.; Lee, J.-H.; Min, B.-W.; Lee, T. Proton irradiation energy dependence of defect formation in graphene. *Appl. Surf. Sci.* **2015**, *344*, 52–56. [CrossRef]
33. Shi, T.; Peng, Q.; Bai, Z.; Gao, F.; Jovanovic, I. Proton irradiation of graphene: Insights from atomistic modeling. *Nanoscale* **2019**, *11*, 20754–20765. [CrossRef] [PubMed]
34. Bel, T.; Muhammettursun, M.; Kocacinar, E.; Erman, E.; Gul, F.B.; Dogan, E.; Celep, M.; Baydogan, N. Improvement of thermal stability and gamma-ray absorption in microwave absorbable poly(methyl methacrylate)/graphene nanoplatelets nanocomposite. *J. Appl. Polym. Sci.* **2021**, *138*, 50897. [CrossRef]
35. Borjanović, V.; Bistričić, L.; Pucić, I.; Mikac, L.; Slunjski, R.; Jakšić, M.; McGuire, G.; Stanković, A.T.; Shenderova, O. Proton-radiation resistance of poly(ethylene terephthalate)–nanodiamond–graphene nanoplatelet nanocomposites. *J. Mater. Sci.* **2016**, *51*, 1000–1016. [CrossRef]
36. Huang, H.; Tang, X.; Chen, F.; Gao, F.; Peng, Q.; Ji, L.; Sun, X. Self-healing mechanism of irradiation defects in nickel–graphene nanocomposite: An energetic and kinetic perspective. *J. Alloys Compd.* **2018**, *765*, 253–263. [CrossRef]
37. Huang, H.; Tang, X.; Chen, F.; Liu, J.; Sun, X.; Ji, L. Radiation tolerance of nickel–graphene nanocomposite with disordered graphene. *J. Nucl. Mater.* **2018**, *510*, 1–9. [CrossRef]
38. Paddubskaya, A.; Batrakov, K.; Khrushchinsky, A.; Kuten, S.; Plyushch, A.; Stepanov, A.; Remnev, G.; Shvetsov, V.; Baah, M.; Svirko, Y.; et al. Outstanding Radiation Tolerance of Supported Graphene: Towards 2D Sensors for the Space Millimeter Radioastronomy. *Nanomaterials* **2021**, *11*, 170. [CrossRef]
39. Cucinotta, F.A. Review of NASA approach to space radiation risk assessments for Mars exploration. *Health Phys.* **2015**, *108*, 131–142. [CrossRef]
40. Zerbi, G.; Gallino, G.; Del Fanti, N.; Baini, L. Structural depth profiling in polyethylene films by multiple internal reflection infra-red spectroscopy. *Polymer* **1989**, *30*, 2324–2327. [CrossRef]
41. Abbate, S.; Gussoni, M.; Zerbi, G. Infrared and Raman intensities of polyethylene and perdeuteropolyethylene: Factor group splittings. *J. Chem. Phys.* **1979**, *70*, 3577–3585. [CrossRef]

42. Mirabella, F.M.; Bafna, A. Determination of the crystallinity of polyethylene/α-olefin copolymers by thermal analysis: Relationship of the heat of fusion of 100% polyethylene crystal and the density. *J. Polym. Sci. Part B Polym. Phys.* **2002**, *40*, 1637–1643. [CrossRef]
43. Owens, D.K.; Wendt, R.C. Estimation of the surface free energy of polymers. *J. Appl. Polym. Sci.* **1969**, *13*, 1741–1747. [CrossRef]
44. Mignot, C. Color (and 3D) for Scanning Electron Microscopy. *Microsc. Today* **2018**, *26*, 12–17. [CrossRef]
45. Yue, L.; Pircheraghi, G.; Monemian, S.A.; Manas-Zloczower, I. Epoxy composites with carbon nanotubes and graphene nanoplatelets—Dispersion and synergy effects. *Carbon* **2014**, *78*, 268–278. [CrossRef]
46. Gulmine, J.V.; Janissek, P.R.; Heise, H.M.; Akcelrud, L. Polyethylene characterization by FTIR. *Polym. Test.* **2002**, *21*, 557–563. [CrossRef]
47. Gaska, K.; Xu, X.; Gubanski, S.; Kádár, R. Electrical, Mechanical, and Thermal Properties of LDPE Graphene Nanoplatelets Composites Produced by Means of Melt Extrusion Process. *Polymers* **2017**, *9*, 11. [CrossRef]
48. Tarani, E.; Arvanitidis, I.; Christofilos, D.; Bikiaris, D.N.; Chrissafis, K.; Vourlias, G. Calculation of the degree of crystallinity of HDPE/GNPs nanocomposites by using various experimental techniques: A comparative study. *J. Mater. Sci.* **2023**, *58*, 1621–1639. [CrossRef]
49. Zakiyan, S.E.; Azizi, H.; Ghasemi, I. Influence of chain mobility on rheological, dielectric and electromagnetic interference shielding properties of poly methyl-methacrylate composites filled with graphene and carbon nanotube. *Compos. Sci. Technol.* **2017**, *142*, 10–19. [CrossRef]
50. Carmen, A.; Arquímedes, K.; Rosestela, P.; Gema, G.; Nohemy, D.; Jeanette, G.; Yanixia, S. HDPE/HA composites obtained in solution: Effect of the gamma radiation. *Nucl. Instrum. Methods Phys. Res. Sect. B* **2006**, *247*, 331–341. [CrossRef]
51. Khonakdar, H.A.; Jafari, S.H.; Wagenknecht, U.; Jehnichen, D. Effect of electron-irradiation on cross-link density and crystalline structure of low- and high-density polyethylene. *Radiat. Phys. Chem.* **2006**, *75*, 78–86. [CrossRef]
52. Moez, A.A.; Aly, S.S.; Elshaer, Y.H. Effect of gamma radiation on low density polyethylene (LDPE) films: Optical, dielectric and FTIR studies. *Spectrochim. Acta Part A* **2012**, *93*, 203–207. [CrossRef] [PubMed]
53. Sadighzadeh, A.; Azimzadeh Asiabi, P.; Ramazani, A.; Ghoranneviss, M.; Salar Elahi, A. Characterization of Gamma Irradiated Low and High Density Polyethylene Using the FTIR and DSC Technique. *J. Inorg. Organomet. Polym.* **2015**, *25*, 1448–1455. [CrossRef]
54. Kumar, P.; Das, B.; Chitara, B.; Subrahmanyam, K.S.; Gopalakrishnan, K.; Krupanidhi, S.B.; Rao, C.N.R. Novel Radiation-Induced Properties of Graphene and Related Materials. *Macromol. Chem. Phys.* **2012**, *213*, 1146–1163. [CrossRef]
55. Fabbri, P.; Valentini, L.; Bittolo Bon, S.; Foix, D.; Pasquali, L.; Montecchi, M.; Sangermano, M. In-situ graphene oxide reduction during UV-photopolymerization of graphene oxide/acrylic resins mixtures. *Polymer* **2012**, *53*, 6039–6044. [CrossRef]
56. Lu, P.; Wu, M.; Ni, Z.; Huang, G. Oxidative degradation behavior of irradiated GO/UHMWPE nanocomposites immersed in simulated body fluid. *Polym. Bull.* **2021**, *78*, 5153–5164. [CrossRef]
57. Vijay, A.R.M.; Ratnam, C.T.; Khalid, M.; Appadu, S.; Gupta, T.C.S.M. Effect of radiation on the mechanical, morphological and thermal properties of HDPE/rPTFE blends. *Radiat. Phys. Chem.* **2020**, *177*, 109190. [CrossRef]
58. Pascaud, R.S.; Evans, W.T.; McCullagh, P.J.J.; FitzPatrick, D. Effects of batch to batch variations and test methodology on degree of crystallinity and melting temperature of UHMW-PE as measured by differential scanning calorimetry. *J. Biomed. Mater. Res.* **1996**, *32*, 619–626. [CrossRef]
59. Wróbel, A.M.; Kryszewski, M.; Rakowski, W.; Okoniewski, M.; Kubacki, Z. Effect of plasma treatment on surface structure and properties of polyester fabric. *Polymer* **1978**, *19*, 908–912. [CrossRef]
60. Abdul-Kader, A.M.; Turos, A.; Radwan, R.M.; Kelany, A.M. Surface free energy of ultra-high molecular weight polyethylene modified by electron and gamma irradiation. *Appl. Surf. Sci.* **2009**, *255*, 7786–7790. [CrossRef]
61. Akbaba, U. Proton and electron irradiation effects on multi-walled carbon nanotubes. *Mater. Res. Express* **2019**, *6*, 075046. [CrossRef]